# Constraints on the Slip Distribution of the 1938 MW 8.3 Alaska Peninsula Earthquake from Tsunami Modeling

Jeffrey Todd Freymueller[1], Elena Suleimani[2], and Dmitry J Nicolsky[3]

[1]Michigan State University
[2]Geophysical Institute, University of Alaska Fairbanks
[3]University of Alaska Fairbanks

November 24, 2022

## Abstract

We simulated tsunami propagation for several scenario slip distributions for the 1938 $M_W$ 8.3 earthquake along the Alaska Peninsula, and compared these to the observed records at Unalaska/Dutch Harbor and Sitka. The Sitka record is sensitive to the depth of slip but not the along-strike location, and is fit best by slip at shallow depth. The Unalaska record is sensitive mainly to the along-strike location of slip, and is fit best by slip that is concentrated in the eastern part of the presumed 1938 rupture zone. The tsunami data show that the actual 1938 earthquake rupture zone was smaller than previously thought, likely ~200 km in length, and had no slip near the Shumagin Islands or in the 2020 Simeonof earthquake's rupture zone. The rupture models that best predict the 1938 tsunami lie within the region of high present day slip deficit inferred from GPS.

1

# Constraints on the Slip Distribution of the 1938 $M_W$ 8.3 Alaska Peninsula Earthquake from Tsunami Modeling

**Jeffrey T. Freymueller[1], Elena N. Suleimani[2], and Dmitry J. Nicolsky[2]**

[1]Department of Earth and Environmental Sciences, Michigan State University, East Lansing, MI, USA.

[2]Geophysical Institute, University of Alaska Fairbanks, Fairbanks, AK, USA.

Corresponding author: Jeffrey T. Freymueller (freymuel@msu.edu)

**Key Points:**

- The 1938 $M_W$ 8.3 Alaska Peninsula earthquake ruptured at shallow depth, within the region of high interseismic slip deficit.
- Slip was confined to the eastern part of the previously inferred rupture zone, and did not overlap with the 2020 Simeonof rupture.
- The 1938 rupture zone was smaller than previously thought, likely no more than ~200 km long

**Abstract**

18 We simulated tsunami propagation for several scenario slip distributions for the 1938 $M_W$ 8.3
19 earthquake along the Alaska Peninsula, and compared these to the observed records at
20 Unalaska/Dutch Harbor and Sitka. The Sitka record is sensitive to the depth of slip but not the
21 along-strike location, and is fit best by slip at shallow depth. The Unalaska record is sensitive
22 mainly to the along-strike location of slip, and is fit best by slip that is concentrated in the eastern
23 part of the presumed 1938 rupture zone. The tsunami data show that the actual 1938 earthquake
24 rupture zone was smaller than previously thought, likely ~200 km in length, and had no slip near
25 the Shumagin Islands or in the 2020 Simeonof earthquake's rupture zone. The rupture models
26 that best predict the 1938 tsunami lie within the region of high present day slip deficit inferred
27 from GPS.

**Plain Language Summary**

29 Earthquakes are a result of slip (a permanent shift) along a fault, or a break within the Earth.
30 Determining the spatial extent of slip in old earthquakes is important, but difficult to do. We used
31 records of the tsunami caused by a 1938 earthquake offshore of the Alaska Peninsula to
32 determine that the earthquake slip was confined to shallow depth, and that the slip on the fault
33 mostly happened at the eastern edge of what had been traditionally drawn as the rupture zone.
34 We found that the earthquake involved a smaller area than previously thought, and that the
35 rupture zone for the 1938 earthquake did not overlap at all with that of the recent 2020 Simeonof
36 earthquake.

**1 Introduction**

38     The seismic and tsunamigenic potential of subduction zones varies from subduction zone
39 to subduction zone, and from location to location within a given subduction zone. The potential
40 for future earthquakes can be assessed if we know the history of slip in past earthquakes and the
41 distribution of *slip deficit*, where the slip deficit is the difference between the plate motion rate
42 (and thus long-term slip rate) and the short-term slip rate of aseismic creep. To a simple first-
43 order approximation, slip that does not occur steadily by aseismic creep or as part of transient
44 slow slip events is likely to occur at a later time as coseismic slip in an earthquake [e.g., Savage,
45 1983; Freymueller et al., 2008; Freymueller, 2020]. The megathrust along the Alaska Peninsula
46 was the location of a 1938 $M_W$ 8.2-8.3 earthquake (Figure 1), and shows strong along-strike
47 variations in slip deficit [*Fournier and Freymueller*, 2008; *Li and Freymueller*, 2018; *Drooff and*
48 *Freymueller*, 2021]. The western end of the Alaska Peninsula is the location of the Shumagin
49 seismic gap [*McCann et al.*, 1979; *Davies et al.*, 1981].

50     The 1938 $M_W$8.3 earthquake occurred along the Alaska Peninsula, east of the Shumagin
51 Islands (Figure 1). *Sykes* [1971] and *Davies et al.* [1981] estimated the rupture area primarily
52 based on the extent of aftershocks, but many of the aftershock locations are highly uncertain
53 (~100 km), as is the mainshock location. *Estabrook et al.* [1994] determined the rupture duration
54 and directivity of the event, and *Johnson and Satake* [1994] modeled the tsunami generated by
55 the event. These sources found that the 1938 earthquake had average slip of 1.8-4 meters, low
56 slip given its presumed rupture area and equivalent to no more than ~75 years of plate motion. In
57 July 2020, an M7.8 megathrust earthquake ruptured the western end of the 1938 segment as it is
58 usually drawn, along with a portion of the Shumagin seismic gap (Figure 1), from ~30-45 km
59 depth [*Crowell and Melgar*, 2020].

Recent paleoseismic studies provide information from just outside both ends of the 1938 rupture zone. *Briggs et al.* [2014] studied a site on Sitkinak Island, at the western end of the 1964 rupture and east of the presumed eastern limit of the 1938 rupture. Sitkinak has experienced both coseismic uplift and subsidence events. *Witter et al.* [2014] analyzed a depositional record on Simeonof Island in the Shumagin islands, west of the 1938 rupture, which showed evidence for a lack of major post-deglaciation tsunamis. Neither site showed measurable land-level change or a tsunami deposit in 1938.
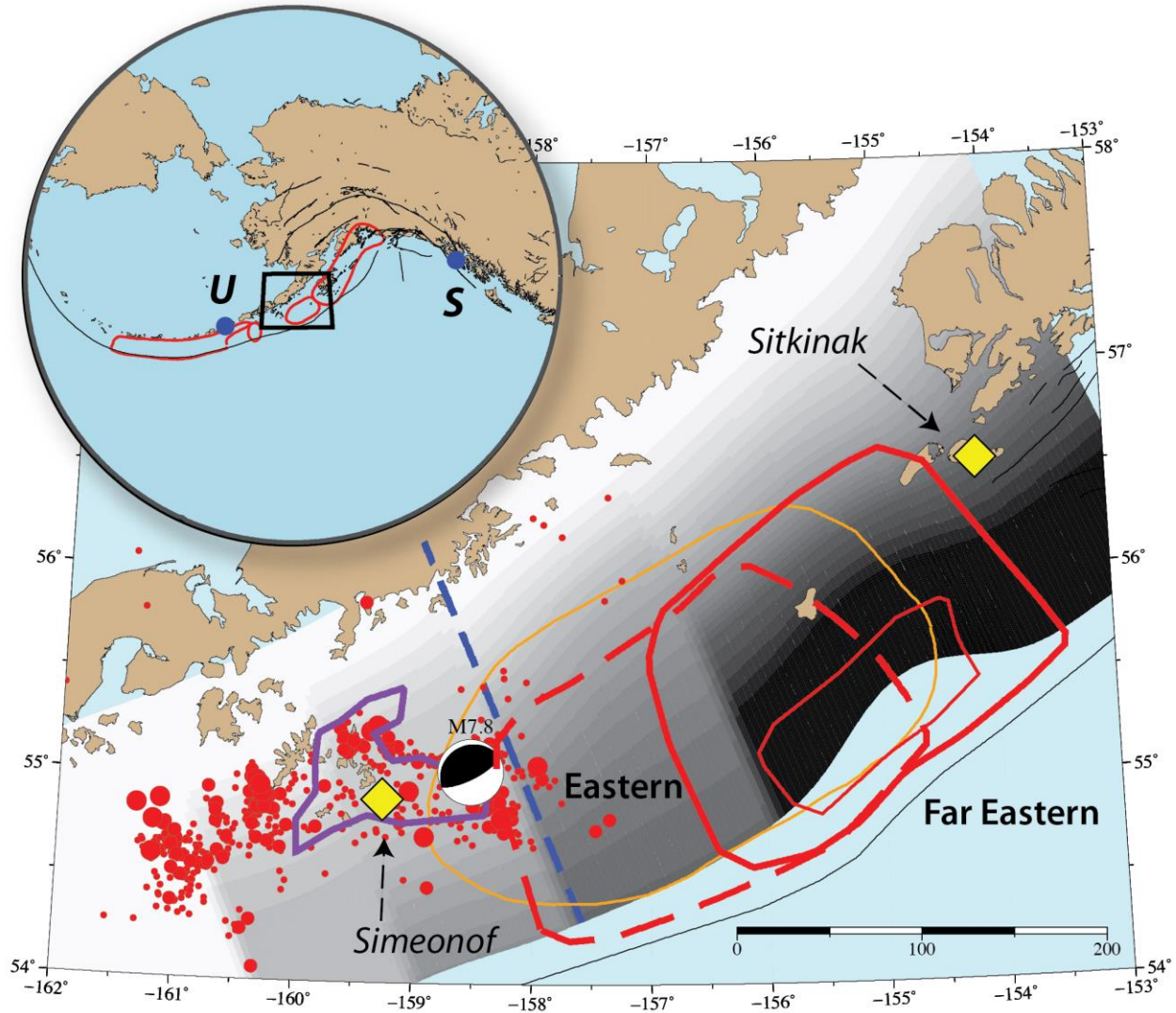


*Figure 1. Location map showing the plate interface, with earthquake rupture zones, and the interseismic slip deficit model of Drooff and Freymueller [2021] in gray shading with darker colors indicating higher slip deficit. The dashed blue line shows the boundary between the segments with wide areas of high slip deficit east of the line, and the largely creeping segments of the Shumagin Gap. The traditionally drawn 1938 outline is shown in orange. The solid red lines are the 1m and 2.5m slip contours from the best-fitting shallow far eastern model, and the dashed red outline is the 1m slip contour for the shallow eastern model. The mainshock (beachball), aftershocks, and 1m slip contour [Crowell and Melgar, 2020] (purple) of the 2020 M7.8 earthquake are shown. The locations of paleo-tsunami sites on Simeonof and*

*Sitkinak islands are shown by yellow diamonds. The inset shows the locations of the Unalaska (U) and Sitka (S) tide gauge stations along with earthquake rupture zones.*

Constraints on the slip distribution are limited. The moment and source-time function for the earthquake are well constrained for such an old event, but the rupture area assumed by both *Johnson and Satake* [1994] and *Estabrook et al.* [1994] was based mainly on contemporary assumptions about the extent of the seismogenic zone. *Johnson and Satake* [1994] assumed a deep rupture, because the observed tsunami was relatively small, but their assumed fault geometry is inconsistent with our present knowledge of the plate interface, having too steep a dip angle and too great a depth (10° dip, shallowest rupture at 20 km depth), and their slip model required slip to be almost entirely downdip of the region of interseismic slip deficit [*Fournier and Freymueller*, 2007; *Li and Freymueller*, 2018; *Drooff and Freymueller*, 2021]. In this study, we test slip models for the 1938 earthquake based on modern estimates of the plate geometry, and the insights gained from geodetic studies of the interseismic slip deficit.

## 2 Data and Modeling Approach

The 1938 tsunami was recorded on tide gauges in Alaska, North America, Hawaii and Japan [*Neumann*, 1940; *Johnson and Satake*, 1994; *Lander*, 1996]. To compare numerical modeling results with observations, we used records from Unalaska and Sitka, which were the closest tide stations to the 1938 tsunami source area. Unfortunately, the original marigrams of the 1938 earthquake have been lost and are no longer available. *Johnson and Satake* [1994] had digitized the original marigrams, but the figures in their paper lacked key timing markers and digital files also were lost. We used the Unalaska record as digitized by the National Geophysical Data Center from the *Lander* [1996] paper. For Sitka, we digitized the record plotted by *Johnson and Satake* [1994], and used images of the marigrams with the documented arrival times from *Neumann* [1940] to constrain the timing of the record. It is likely that the timing of the records has an uncertainty of about 5 min.

To simulate ruptures on the Aleutian megathrust we employed the Slab2.0 model for the geometry of the Alaska–Aleutian plate interface [*Hayes et al.*, 2018; *Hayes*, 2018]. We finely discretized the Slab2.0 model to construct a high resolution geometric model of the interface that using rectangular sub-faults that are consistent with the *Okada* [1985] requirements (Figure S1). The upper and lower edges of each sub-fault coincide with depth contours of the plate interface spaced at 1 km, and the rectangles ranged from 3 to 6 km length in the along-strike direction. Slip scenarios, as detailed below, were mapped onto this high resolution geometric model to compute the coseismic ground deformation [*Okada*, 1985]. We then simulated the resulting tsunami using the vertical coseismic displacements as the initial conditions, to determine the sensitivity of the tsunami time series at Unalaska and Sitka to different slip patterns.

We generated slip scenarios by multiplying a function $f(x)$ describing the along-strike distribution of slip and a function $g(y)$ describing the downdip distribution (Figure 2). The approach is similar to that used by *Nicolsky et al.* [2016] except that we applied the slip variation equations of *Freund and Barnett* [1976] to the entire rupture area to generate smooth, tapered slip distributions. The two functions were varied to generate a grid of 9 different slip distributions, and we generated the tenth, the shallow far eastern model, by shifting the slip distribution of the shallow eastern model to the east. All sources were scaled to have the same seismic moment, equivalent to $M_W$ 8.25.
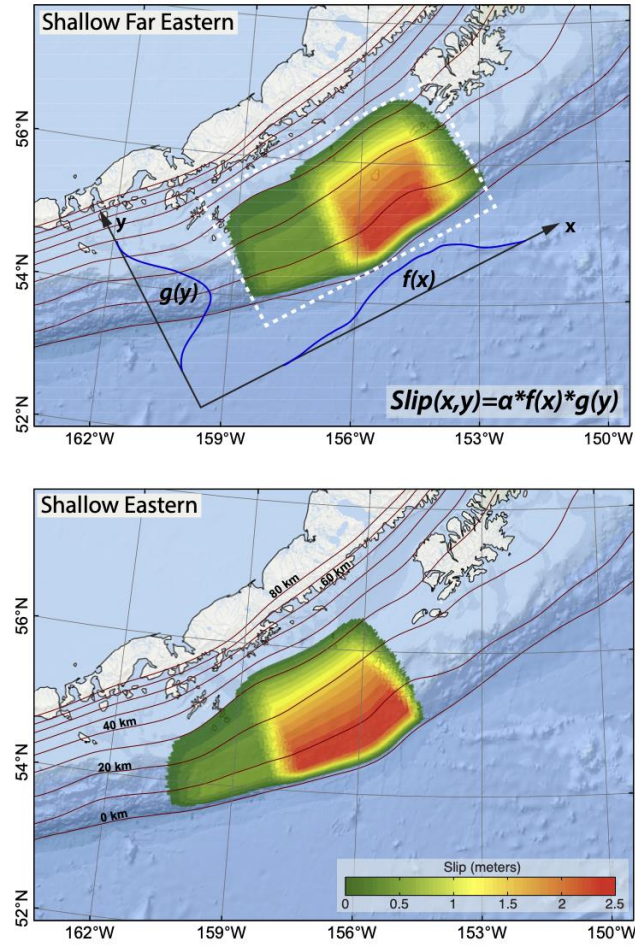
120

*Figure 2. Example slip distributions for two of the slip models, shallow eastern and shallow far eastern. For each model the slip is the product of a function f(x) representing the along-strike variation and g(y) representing the downdip variation, and then scaled to a constant magnitude M_W 8.25. The functions f(x) and g(y) are based on relations in Freund and Barnett [1976]. For the central and western models, the rupture area is the same as for the eastern model, but the area of higher slip is shifted to the west. For the mid-depth and deep models, the main area of high slip is shifted downdip.*

In the downdip direction, we specified three rupture types: "shallow" (trench to ~30 km depth), "mid-depth" (~20-40 km depth), and "deep" (~30-50 km depth). The shallow rupture corresponds to the geodetically inferred locked area of *Fournier and Freymueller* [2007], which considered a region of uniform slip deficit. Li and Freymueller [2018] developed a slip deficit model with downdip smoothing, which showed that a gradual decrease of slip deficit with depth also fits the data. The mid-depth model spans a partially locked area with slip deficit decreasing with depth, and also approximates the horizontal position of the rupture model of *Johnson and Satake* [2004]. A deep rupture model also is considered for completeness.

In the along-strike direction, we generated models with slip along 3 overlapping ranges, with the slip concentrated either at the western end of the region, in the middle of it, or at its eastern end. The western models have slip concentrated within the Shumagin gap, the middle models have slip concentrated in the western part of the inferred 1938 aftershock zone, and the

140 eastern models have slip concentrated in the eastern part of the aftershock zone. Varying the slip
141 along strike for each of the three depth intervals, we constructed nine different source slip
142 distributions, all with equal moment. We also considered a far eastern model in which we shifted
143 the shallow eastern source along strike to the east. Figure 3 shows the coseismic vertical seafloor
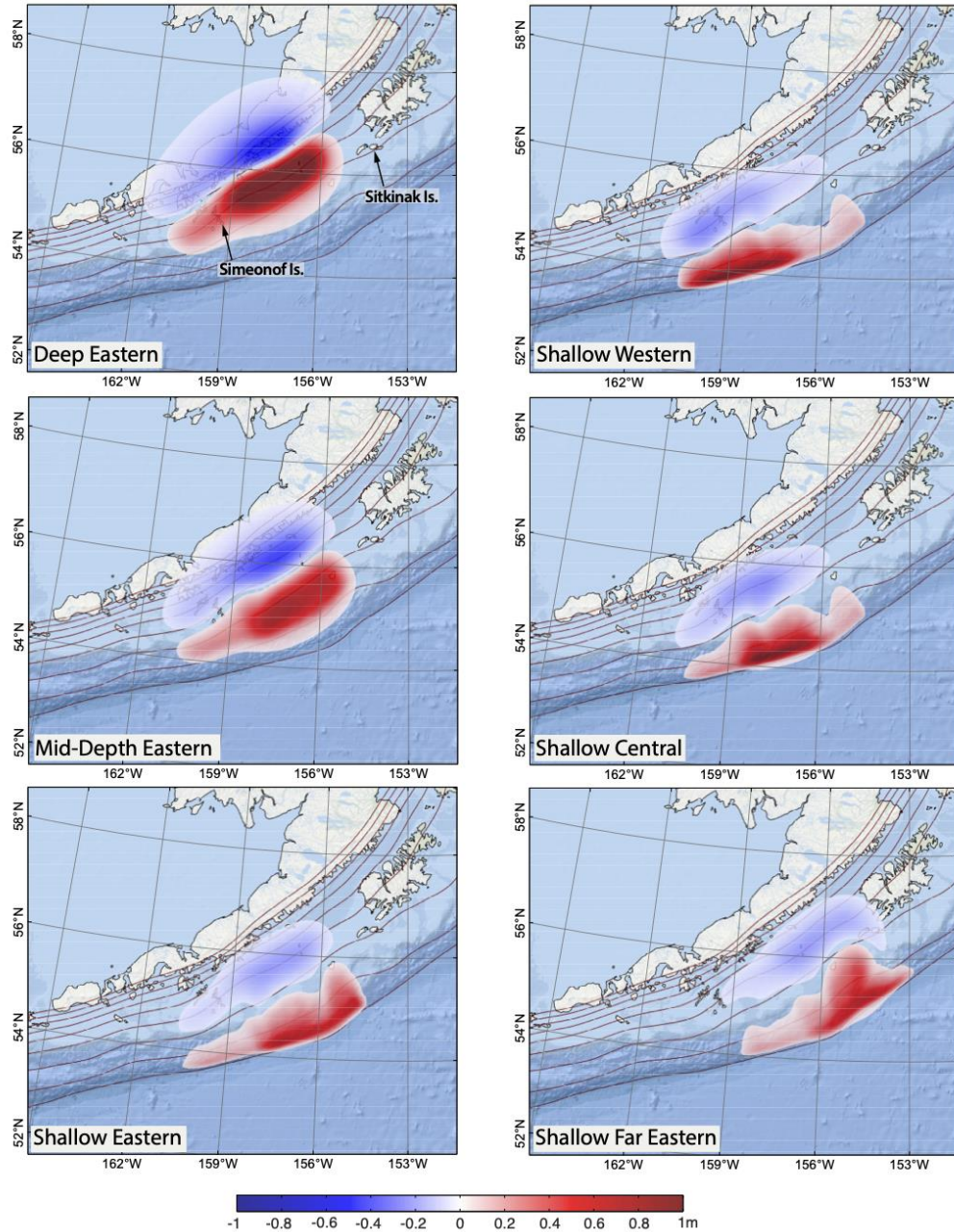144 displacement for several of these rupture scenarios.



145

146 *Figure 3. Vertical seafloor displacements caused by representative slip scenarios. On the left*
147 *side, the slip is concentrated in the east and the deep, mid-depth and shallow slip distribution*
148 *scenarios are shown. On the right, the Western, Central and Far Eastern slip distribution*
149 *scenarios are shown assuming the shallow rupture. Displacements are in meters. Red*
150 *contours show depth to the plate interface from 0 to 80 km with a 10 km increment.*

151   There is considerable uncertainty in the seismic moment for such an old event, and an
152 error in moment maps linearly into an error in average slip, and thus tsunami amplitude. In
153 converting moment to slip, we assumed a shear modulus of 36 GPa. We used $M_W$ 8.25 model
154 events, in the middle of of the range of estimated event magnitudes. Models that overpredict or
155 underpredict the observed tsunami by up to a factor of 1.5 could easily be reconciled by
156 adjusting the moment by ±0.05 units. The relative heights of different peaks are a more robust
157 measure of model fit to the data than absolute amplitude. Arrival time mismatches of several
158 minutes or less cannot be distinguished from timing errors in the data, but much larger arrival
159 time discrepancies or a mismatch in the time between successive peaks indicate a model that fits
160 the data poorly.

161   For each modeled slip distribution on the plate interface, we simulated the propagation of
162 the resulting tsunami to Unalaska and Sitka using the *Nicolsky et al.* [2011] numerical model of
163 tsunami propagation and runup. The model solves flux-based nonlinear shallow-water equations
164 in spherical coordinates, which was verified and validated using a series of analytical, laboratory
165 and field benchmarks [*Nicolsky et al.*, 2011]. Additionally, the model was successfully tested to
166 model propagation of the 2011 Tohoku transoceanic tsunami at the DART buoys located next to
167 Unalaska [*Nicolsky et al.*, 2015]. We used a series of nested bathymetric grids of with increasing
168 spatial resolution in shallower water, as described in *Nicolsky et al.* [2016].

**3 Results**

169

170   Figure 4 shows comparisons between the simulated time series for 10 tsunami sources
171 (western, middle, and eastern; shallow, mid-depth, and deep; plus the shallow far eastern source)
172 and the observed tsunami at Sitka and Unalaska. The Sitka records have little sensitivity to the
173 location of slip, but are very sensitive to the depth. Only the shallow sources fit the data at Sitka
174 well, and these are an excellent match for the observed arrival time. As the source depth is
175 increased the mismatch in the arrival time becomes significant, and relative amplitudes of the
176 two peaks become more different; the data show two peaks of almost the same amplitude. The
177 first arriving peak is too small in the deeper source models, likely because of the smaller initial
178 seafloor displacement. The timing of the second peak in all the models matches the arrival time
179 of a low, broad, second peak that travels from the source, but the amplitude seems to be
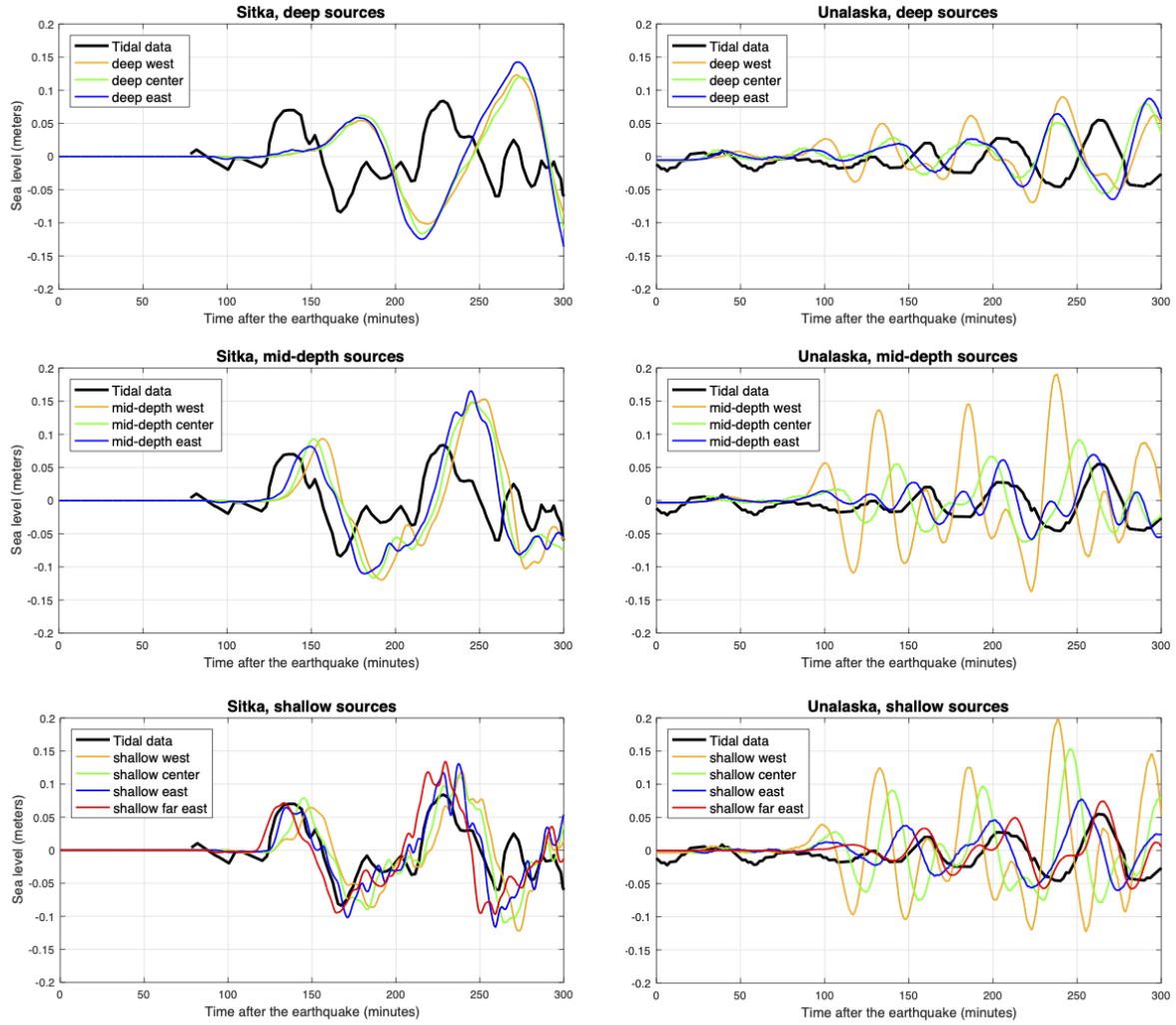180 controlled mainly by local effects (see Movies S1 and S2).

181

*Figure 4. Tide gauge data from the Sitka tide gauge (left) and the Unalaska tide gauge (right), with predictions from the full range of models (west, middle, and eastern sources, at three different depth ranges). The far eastern source is shown as well among the shallow sources.*

Because Unalaska is much closer to the source area than Sitka, it is more sensitive to the along-strike variations in the slip distribution, as the travel path is dominantly along the subduction zone. The predicted waveforms for the deep sources disagree with the observations, arriving substantially early. The mid-depth sources fit reasonably well for the eastern model, but the western and central models have larger amplitudes, different waveform shapes, and arrive too early. For the shallow sources, the eastern and far eastern models reproduce the basic character of the observations, while the western and central models have amplitudes much too large and double troughs in the model waveforms that are not observed in the data.
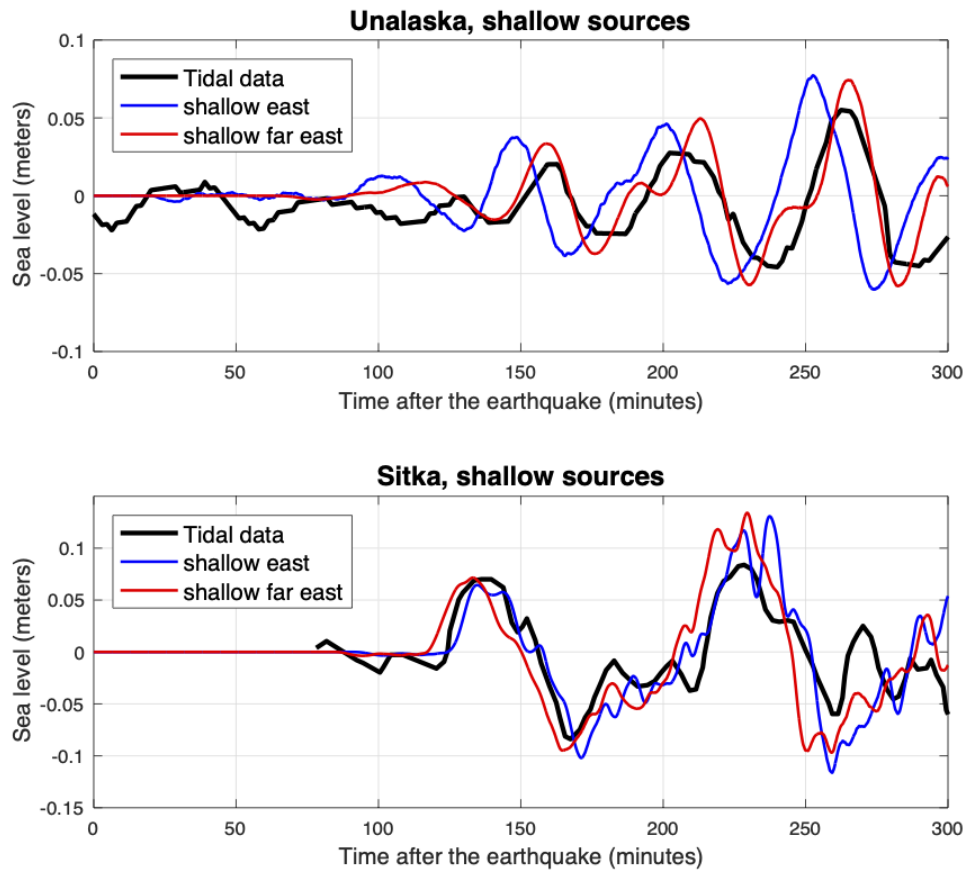
*Figure 5. Tide gauge data and model predictions for the eastern and far eastern source models.*

Figure 5 shows a closer comparison of the shallow eastern and far eastern models. The far eastern model is a better fit to the data, although the eastern model is also a reasonable fit. The simulated waveforms are very similar at Sitka, with difference in arrival times not significant given the timing uncertainty. The simulated time series at Unalaska differ mainly in arrival time, with the far eastern source better matching the timing of the peaks and the eastern source arriving ~15 min early, a mismatch about three times larger than the estimated timing uncertainty. *Nicolsky et al.* [2015] found a similar timing mismatch at Unalaska for models of the 1957 tsunami, so errors in modeling the propagation might explain the mismatch. Both models slightly overestimate the amplitude, suggesting a magnitude slightly lower than $M_W$ 8.25. Clearly, slip in 1938 was heavily concentrated in the eastern end of its presumed rupture zone, and might extend east of the presumed rupture zone, where it would directly abut the 1964 earthquake rupture. This result is similar to that of *Johnson and Satake* [1994]. Models involving slip west of the main slip region of the eastern model can be ruled out.

The shallow far eastern model predicts that there was ~6 cm of subsidence at Sitkinak Island, which is too small to have left a clear geologic record. Sitkinak Island also subsided in 1964 [*Briggs et al.*, 2014].

**4 Discussion**

The tsunami observations show that slip on the western half of the 1938 rupture zone as traditionally drawn must have been much smaller than the slip in the eastern half, and the tsunami can be explained adequately with little to no slip in that part of the rupture. The far eastern model features coseismic slip that is mostly located within the most strongly locked interseismic segment. That model and the eastern model both have all or nearly all of their rupture area located in the wide locked region (east of the blue dashed line on Figure 1), and essentially no slip in the largely creeping segments west of there. Our results suggest that the rupture zone of the 2020 Simeonof earthquake did not slip at all in 1938 (Figure 1), as the rupture zones did not overlap either along strike or in depth. Thus it is possible that 2020-sized events could occur downdip of the 1938 rupture, and 1938-like events could occur updip of the 2020 rupture, if there are large-enough regions of slip deficit there.

Comparison of these coseismic models to the interseismic model (Figure 1) shows that the the inferred 1938 rupture area lies within the area of estimated present-day interseismic slip deficit, both downdip and along-strike. The interseismic data can be fit either by models with a gradual [Li and Freymueller, 2018; *Drooff and Freymueller*, 2021] or an abrupt [*Fournier and Freymueller*, 2007] downdip decrease in slip deficit, but the high slip zone in our slip models lies within the locked zone in either case. These interseismic models lack resolution for the slip deficit near the trench, and did not estimate a value for depths shallower than 10 km, so the updip slip limits cannot be compared. The low average slip in 1938 and depth extent smaller than the interseismic locked zone also raises the possibility that much larger events could occur, rupturing both the shallow and deeper parts of the inferred interseismic locked region.

Our slip models suggest that the 1938 rupture was shorter along-strike than has been assumed previously based on aftershocks, likely ~200 km long rather than ~275-300 km, and the high slip area was much smaller than the traditionally drawn rupture zone. Our modeling confirms the previous findings that the 1938 event was a low slip event relative to its rupture dimensions. The peak slip in our models is only slightly larger than the peak slip in the 2020 M7.8 Simeonof event [*Crowell and Melgar*, 2020], although the rupture area was much larger. It is possible that the actual rupture was more compact with higher average slip than in our models. Given the differences and similarities in fit to the data for the suite of models we tested, we do not think that the available tsunami data can distinguish between a rupture model like those shown here and a more compact model with higher average slip. A more compact model would have a higher average slip, and correspondingly longer recurrence time, but  would also leave a larger part of the interface unruptured over the last century, with a larger accumulated slip deficit.

It can be misleading to equate the aftershock zones of old earthquakes with the rupture zone. For one thing, the uncertainties in the locations of the 1938 mainshock and aftershocks are very large, so it is likely that the aftershock zone would appear larger than the actual slip zone. In addition, the aftershock region of the 2020 M7.8 event (Figure 1) was substantially larger than the slip zone. Vigorous aftershocks from that event extended nearly 100 km west of the main 2020 slip zone, and given the proximity of the 1938 and 2020 ruptures, it is possible that the same was true in 1938, as the entire region west of the 1938 rupture is dominated by creep.

## 5 Conclusions

The 1938 Alaska Peninsula tsunami was recorded at tide gauges in Sitka and Unalaska, each of which places distinct constraints on the earthquake slip distribution. The Sitka tide gauge record is matched only by models with the slip confined to shallow depths, while the Unalaska tide gauge record is matched only if slip in the event was confined to the eastern part of the aftershock zone as it has been traditionally drawn. Thus, slip in the 1938 earthquake was confined to shallow depths and to the eastern part of what had previously been considered its rupture zone; the tsunami data are best fit by a model in which the main slip patch is at the far eastern end of the rupture. We can fit the tsunami data well with models that have peak slip of less than ~3 m, only slightly larger than the peak slip of the much smaller 2020 event. This is consistent with previous results for the 1938 rupture, which also had low average slip. Our models for the 1938 earthquake have slip that lies entirely within the zone of  interseismic slip deficit.

The tsunami data show that the actual 1938 earthquake rupture zone was smaller than had been previously thought, likely ~200 km in length, and had little or no slip near the Shumagin Islands. The 1938 slip region almost certainly did not overlap with any part of the 2020 Simeonof earthquake's rupture zone. The main slip zone in 1938 was restricted to shallow depths, and the main slip zone was likely limited to depths entirely shallower than the 2020 rupture. These results permit a scenario in which 2020-like events could occur downdip of our inferred 1938 rupture, or a 1938-like event could occur updip of the 2020 earthquake, if there was sufficient slip deficit.

## Acknowledgments, Samples, and Data

## References

Briggs, R. W., S. E. Engelhart, A. R. Nelson, T. Dura, A. C. Kemp, P. J. Haeussler, D. R. Corbett, S. J. Angster, & L.-A. Bradley (2014), Uplift and subsidence reveal a nonpersistent megathrust rupture boundary (Sitkinak Island, Alaska), *Geophysical Research Letters*, 41, 2289–2296, doi:10.1002/2014GL059380.

Crowell, B. W., & Melgar, D. (2020), Slipping the Shumagin Gap: A kinematic coseismic and early afterslip model of the Mw 7.8 Simeonof Island, Alaska, earthquake. *Geophysical Research Letters*, 47, e2020GL090308. https://doi.org/10.1029/2020GL090308.

Davies, J., L. Sykes, L. House, & K. Jacob, Shumagin seismic gap (1981), Alaska Peninsula history of great earthquakes, tectonic setting and evidence for high seismic potential, *J. Geophys. Res.*, 86, 3821–3855.

Drooff, C., & J. T. Freymueller (2021), New Constraints on Slip Deficit on the Aleutian Megathrust and Inflation at Mt. Veniaminof, Alaska from Repeat GPS Measurements. *Geophysical Research Letters*, https://doi.org/10.1029/2020GL091787.

Estabrook, C. H., Jacob, K. H., & Sykes, L. R. (1994), Body wave and surface wave analysis of large and great earthquakes along the Eastern Aleutian Arc, 1923–1993: Implications for future events. Journal of Geophysical Research, 99, 11,643–11,662. https://doi-org/10.1029/93JB03124.

Fournier, T. J., & J. T. Freymueller (2007), Transition from locked to creeping subduction in the Shumagin region, Alaska, *Geophysical Research Letters*, 34, L06303, doi:10.1029/2006GL029073.

Freund, L.B., & Barnett, D.M. (1976), A two-dimensional analysis of surface deformation due to dip-slip faulting: Bulletin of the Seismological Society of America, v. 66, p. 667–675.

Freymueller, J. T., (2020), GPS – Tectonic Geodesy, in *Encyclopedia of Solid Earth Geophysics*, 2nd ed., H. Gupta, ed., Springer-Verlag, https://doi.org/10.1007/978-3-030-10475-7_77-1.

Freymueller, J.T., H. Woodard, S. Cohen, R. Cross, J. Elliott, C. Larsen, S. Hreinsdóttir, & C. Zweck (2008), Active deformation processes in Alaska, based on 15 years of GPS measurements, in *Active Tectonics and Seismic Potential of Alaska,* AGU Geophysical Monograph, 179, J.T. Freymueller, P.J. Haeussler, R. Wesson, and G. Ekstrom, eds., pp. 1-42, AGU, Washington, D.C.

Hayes, G. (2018), Slab2 - A Comprehensive Subduction Zone Geometry Model: U.S. Geological Survey data release, https://doi.org/10.5066/F7PV6JNV.

Hayes, G. P., G. L. Moore, D. E. Portner, M. Hearne, H. Flamme, M. Furtney, & G. M. Smoczyk (2018), Slab2, a comprehensive subduction zone geometry model. *Science*, 362, pp. 58-61, DOI: 10.1126/science.aat4723.

Johnson, J. M., & K. Satake (1994), Rupture extent of the 1938 Alaskan earthquake as inferred from tsunami waveforms, Geophys. Res. Lett., 21, 733-736.

Lander, J.F. (1996), Tsunamis affecting Alaska, 1737–1996: Boulder, CO, National Oceanic and Atmospheric Administration, National Geophysical Data Center (NGDC), Key to Geophysical Research Documentation, v. 31, 155 p.

Li, S., & Freymueller, J. T. (2018), Spatial variation of slip behavior beneath the Alaska Peninsula along Alaska-Aleutian subduction zone. *Geophysical Research Letters*, *45*. https://doi.org/10.1002/ 2017GL076761.

McCann, W.R., S. P. Nishenko, L.R. Skyes, & J. Krause (1979), Seismic gaps and plate tectonics: seismic potential of major boundaries, Pure Appl. Geophys., 117, 1082-1147, https://doi.org/10.1007/BF00876211.

Neumann, F. (1940), United States Earthquakes, 1938: U.S. Department of Commerce, Coast and Geodetic Survey, Washington, Serial No. 629, 59 p.

Nicolsky, D.J., Suleimani, E.N., & Hansen, R.A. (2011), Validation and verification of a numerical model for tsunami propagation and runup: Pure and Applied Geophysics, v. 168, p. 1,199–1,222. doi:10.1007/s00024-010-0231-9.

336 Nicolsky, D.J., Suleimani, E.N., Freymueller, J.T., & Koehler, R.D. (2015), Tsunami inundation
337 maps of Fox Islands communities, including Dutch Harbor and Akutan, Alaska: Alaska Division
338 of Geological & Geophysical Surveys Report of Investigation 2015-5, 67 p., 2 sheets, scale
339 1:12,500. http://doi.org/10.14509/29414.

340 Nicolsky, D. J., J. T. Freymueller, R. C. Witter, E. N. Suleimani, & R. D. Koehler (2016),
341 Evidence for shallow megathrust slip across the Unalaska seismic gap during the great 1957
342 Andreanof Islands earthquake, eastern Aleutian Islands, Alaska, Geophys. Res. Lett., 43,
343 10,328–10,337, doi:10.1002/2016GL070704.

344 Okada, Y. (1985), Surface deformation due to shear and tensile faults in a half-space: Bulletin of
345 the Seismological Society of America, v. 75, no. 4, p. 1,135–1,154.

346 Savage, J. (1983), A dislocation model of strain accumulation and release at a subduction zone,
347 J. Geophys. Res., 88, 4984–4996.

348 Sykes, L. R. (1971), Aftershock zones of great earthquakes, seismicity gaps, and earthquake
349 prediction for Alaska and the Aleutians, J. Geophys. Res., 76, 8021–8041.

350 Witter, R. C., R. W. Briggs, S. E. Engelhart, G. Gelfenbaum, R. D. Koehler, & W. D. Barnhart
351 (2014), Little late Holocene strain accumulation and release on the Aleutian megathrust below
352 the Shumagin Islands, Alaska, Geophys. Res. Lett., 41, 2359–2367, doi:10.1002/
353 2014GL059393.

354

355     **Figure 1.** Location map showing the plate interface, with earthquake rupture zones, and the
356     interseismic slip deficit model of Drooff and Freymueller (2021) in gray shading with darker
357     colors indicating higher slip deficit. The dashed blue line shows the boundary between the
358     segments with wide areas of high slip deficit east of the line, and the largely creeping segments
359     of the Shumagin Gap. The traditionally drawn 1938 outline is shown in orange. The solid red
360     lines are the 1m and 2.5m slip contours from the best-fitting shallow far eastern model, and the
361     dashed red outline is the 1m slip contour for the shallow eastern model. The mainshock
362     (beachball), aftershocks, and 1m slip contour [Crowell and Melgar, 2020] (purple) of the 2020
363     M7.8 earthquake are shown. The locations of paleo-tsunami sites on Simeonof and Sitkinak
364     islands are shown by yellow diamonds. The inset shows the locations of the Unalaska (U) and
365     Sitka (S) tide gauge stations along with earthquake rupture zones.

366     **Figure 2.** Example slip distributions for the mosaic of sub-events used to construct the slip
367     distribution of larger events. At each grid point (defined by the intersection of a line parallel to
368     depth and a line in the downdip direction, we place a unit slip distribution that is smooth and
369     centered on the grid point. Red colors indicate high slip, and cool colors indicate low slip. Larger
370     slip events can be constructed by scaling and summing these unit sources. Note that only every
371     third source is shown in the downdip direction for clarity.

372     **Figure 3.** Vertical seafloor displacements caused by representative slip scenarios. On the left
373     side, the slip is concentrated in the east and the deep, mid-depth and shallow slip distribution
374     scenarios are shown. On the right, the Western, Central and Far Eastern slip distribution
375     scenarios are shown assuming the shallow rupture. Displacements are in meters. Red contours
376     show depth to the plate interface from 0 to 80 km with a 10 km increment.

377     **Figure 4.** Tide gauge data from the Sitka tide gauge (left) and the Unalaska tide gauge (right),
378     with predictions from the full range of models (west, middle, and eastern sources, at three
379     different depth ranges). The far eastern source is shown as well among the shallow sources.

380     **Figure 5.** Tide gauge data and model predictions for the eastern and far eastern source models.
381